Express Polymer Letters Vol.16, No.12 (2022) 1267–1279
Available online at www.expresspolymlett.com
https://doi.org/10.3144/expresspolymlett.2022.92

Research article

Development of stretchable and bendable polymer wearable antenna for 5G applications

Shakhirul Mat Salleh[1,3], *Mohd Fadzil Ain*[1*], *Zulkifli Ahmad*[2], *Intan Sorfina Zainal Abidin*[1], *Che Muhammad Nor Che Isa*[3]

[1]School of Electrical and Electronic Engineering, Universiti Sains Malaysia, Nibong Tebal, Penang, Malaysia
[2]School of Materials and Mineral Resources Engineering, Universiti Sains Malaysia, Nibong Tebal, Penang, Malaysia
[3]Faculty of Electronic Engineering Technology, Universiti Malaysia Perlis, Pauh Putra Campus, Arau, Perlis, Malaysia

Received 4 April 2022; accepted in revised form 21 July 2022

Abstract. Smart polymer nanocomposite (SPN) is a major interest in the development of wearable electronics, which requires the conductive matrix to be both flexible and stretchable. Polydimethylsiloxane (PDMS) was chosen in this study as it offers flexibility, thermal stability, relative isotropic, homogeneity, low permittivity, and ease of fabrication. The conductive silver paste filler loadings of 40, 50, 60, and 65 wt% were constructed and measured, which showed high conductivity in the range of 1.59–6.58·10^6 S/m. A rectangular microstrip patch antenna was fabricated based on stretchable PDMS substrate and silver paste polysiloxane composite at a resonance frequency of 3.5 GHz for fifth-generation (5G) communication. The proposed antenna was designed to attach to the human body and integrate with a wearable device. The polymer wearable antenna will easily stretch and bend following the human body shape and movements, which was investigated to further understand the antenna performance at different stretching and bending conditions. Furthermore, the specific absorption rate (*SAR*) wearable antenna was analysed for safety purposes.

Keywords: *polymer composites, modelling and simulation, material testing, wearable antenna, stretch/flexible antenna*

1. Introduction

The nature of smart materials has inspired researchers to improve the development of smart polymers in recent years. Smart materials can be defined as materials that incorporate the functions of sensing, actuation, and control [1, 2]. A review [3] has classified smart polymer nanocomposites (SPN) into subcategories; stimuli-active polymers [4, 5], shape memory polymer [6–8], smart electrorheological (ER) and magnetorheological (MR) polymer [9, 10], self-heating polymer [11–13], self-healing polymer [14, 15], self-cleaning polymer [16, 17], self-sensing polymer [18, 19], energy-harvesting, and energy storage polymer [20–22]. Furthermore, the applications of SPNs are widely used in sensors and actuators [23, 24], aircraft and aerospace [25–27], stretchable electronics [28–30], wearable electronics, and smart textile applications [31–34].

This study mainly focused on the development of stretchable and flexible polymer wearable antenna for 5G applications. 5G wearable antennas offer a wide range of usage in people's daily lives. Which include medical applications in addition to wristwatches, exercise bands, and augmented reality glasses [35–37]. In addition, a wearable antenna has been used as a medium for transferring data in healthcare to monitor patient`s critical health conditions, military, as well as for rescue operations [38–40]. Such antennas are mainly attached to the body for a wireless body sensor network, which requires specific considerations, such as lightweight, flexibility, robustness, ease of integration, and comfortable

*Corresponding author, e-mail: eemfadzil@usm.my

to the user, as opposed to rigid conventional antennas. Therefore, the material chosen is the main key in designing a wearable antenna. For example, fabric materials, such as felt, cotton, and denim, are used as antenna substrate, while the conductive fabric, Shieldit Super, and copper sheet are used as a patch and ground of the antenna [41–43] to offer flexibility but is non-stretchable. Thus, polydimethylsiloxane (PDMS) as a substrate has become a popular choice for research purposes, as it offers flexibility and stretchability, subsequently providing a higher degree of freedom or control of user movements. However, previous work by [44, 45] used PDMS substrate embedded with conductive fabric while [46–48] used PDMS-copper foil, which is rigid conductive that will limit the stretchability. Hence, this study used conductive silver-PDMS (Ag-PDMS) formulated paste so it can stretch and be strongly embedded on the PDMS substrate antenna without cracking when subjected to mechanical deformation, such as stretching or bending. On the other hand, the wearable antenna always faces some common problems when attached to the body, where the antenna structure simply deforms to the shape and movement would affect the antenna performance. Therefore, this study also performed an analysis on the wearable antenna in stretching and bending conditions, resulting in the reflection coefficient *S11*, bandwidth, radiation pattern, directivity, gain, and specific absorption rate (*SAR*).

2. Methodology

2.1. Substrate sample preparation

Sylgard 184 (PDMS) consisted of two parts (base and curing agent) and was in a liquid form in its initial stage that was used as a substrate. The substrate sample of 40×40×2 mm^3 was prepared by mixing the two parts in the ratio of 10:1 as suggested by the material provider company [49]. This ratio has also been used by another researcher as a substrate, and it showed good stiffness when stretching, rolling, and twisting [50]. After it was well mixed, the sample was treated under vacuum suction to remove air bubbles and subsequently cured under thermal curing at 100 °C over 35 minutes. The dielectric constant, ε_r', of the substrate was measured using a Keysight 85075E dielectric probe kit from Keysight Technologies at 3.5 GHz, which was 2.74. The details of the parameters obtained are shown in Table 1. The dielectric changed depending on the frequency, temperature, mixture, orientation, pressure, and molecular structure of the material. The dielectric constant, ε_r', is a measure of how much energy was stored in a material from an external electric field and the ability of a material to be polarized by an electric field [51]. The loss factor, ε_r'', is a measure of how lossy or dissipative a material is to an external electric field, also known as the imaginary part of the permittivity [52, 53]. The interactions of electrical property through complex relative permittivity of the material, ε_r, is defined as Equation (1) [54]:

Table 1. The parameters of the substrate (PDMS).

Parameter		Value
Frequency, f	[GHz]	3.5
Dielectric constant, ε_r'	[–]	2.74
Dielectric loss factor, ε_r''	[–]	0.157
Loss tangent, $\tan\delta$	[–]	0.057

$$\varepsilon_r = \varepsilon_r' - j\varepsilon_r'' \tag{1}$$

The electric loss tangent, $\tan\delta$, of the material was also named the dissipation factor, which signified the ratio of the imaginary part (energy loss) to the real part (energy stored) of the complex permittivity, as defined in Equation (2) [54]. All of these parameters are important in formulating and designing the microstrip patch antenna:

$$\tan\delta = \frac{\varepsilon_r''}{\varepsilon_r'} \tag{2}$$

2.2. Conductive silver paste preparation

Applied materials

Five different silver fillers (40, 50, 60, 65, and 70 wt%) were prepared. The silver powder size was 2–3.5 µm. The poly(dimethylsiloxane) hydroxyl (OH-PDMS) that was terminated with an average molecular weight (M_n) of 110·10 g/mol and viscosity of $50 \cdot 10^3$ cSt, cyclotetrasiloxane (D4) functioned as an intermediate, (3-glycidyloxypropyl)-trimethoxysilane (ETMS) and (3-trimethyloxysily) propyl methacrylate (ATMS) functioned as additives, vinyltrimethoxysilane (VTMS) functioned as a coupling agent, and dibutyltin dilaurate (DBDL) functioned as a curing agent. All the materials above were purchased from Sigma Aldrich (USA), except for D4, which was a gift from Penchem Technologies Sdn. Bhd. (Penang, Malaysia).

The fabrication of conductive paste

The OH-PDMS (0.2 g), D4 (250 µl), ETMS, VTMS, ATMS (10 µl each), and Ag powder fillers (40, 50,

60, 65, and 70 wt%) were mixed using a magnetic stirrer for 10 minutes at 210 rpm. The curing agent DBTDL (5 µl) was added to the mixture and stirred momentarily before a squeegee was printed onto the PDMS substrate, as prepared earlier in Section 2.1. The entire package was then thermally cured for 40 minutes at 60 °C to create a conductive strip that can strongly adhere to the stretchable PDMS substrate. It must be noted that unlike the method presented in [50], this paper did not use ultrasonication; as it can break the polymer chain and produce heat that will speed up the curing constantly, thus, causing a reduced working window time, especially during the squeegee printing process. Figure 1 shows the five Ag samples of filler: 40, 50, 60, 65, and 70 wt%. High-resolution patterns can be achieved when Ag fillers between 40–65 wt% are used, as the composite does not flow after removing the stencil due to its high viscosity. However, 70 wt% was the most viscous paste in this group and was difficult to spread thinly, rendering it unsuitable for printing use.

The measurement of the conductivity

The four-point collinear probe measurement method was done using a Keithley 4200A-SCS parameter analyser from Tektronix (Beaverton, USA). This technique involves four equally spaced probes in contact with a material of unknown resistance. The two outer probes are used for sourcing current, and the inner probes are used for measuring the resulting voltage drop across the surface of the sample material. The volume resistivity obtained using Equation (3) [55] has been programmed in the measurement setup:

$$\rho = \frac{\pi}{\ln 2} \cdot \frac{V}{I} \cdot t \tag{3}$$

where ρ is the volume resistivity [Ω·cm], V is the measured voltage [V], I is the source current [A], and t is the sample thickness [cm]. Therefore, the conductivity, σ, of the material can be calculated using Equation (4) [55]:

$$\sigma = \frac{1}{\rho} \tag{4}$$

The measured conductivity at different wt% is presented in Figure 2, which resulted in the high conductivity value compared to other studies [50, 56–59]. The high threshold loading is attributed to the increased conductivity of composite, where the fillers form a continuous network within polymeric matrices and perform better electrical properties. This scenario is similar to that reported in other works [50, 60, 61]. However, apart from the filler loading, the type of materials, size and concentration of reinforcements, dispersion of fillers within a polymeric matrix, and processing techniques also governed the electrical properties of the polymer composite [62].

2.3. Antenna design and fabrication

The microstrip patch antenna was designed at 3.5 GHz for 5G application using Equations (5)–(8) [63]. W is the width, and L is the length of the patch

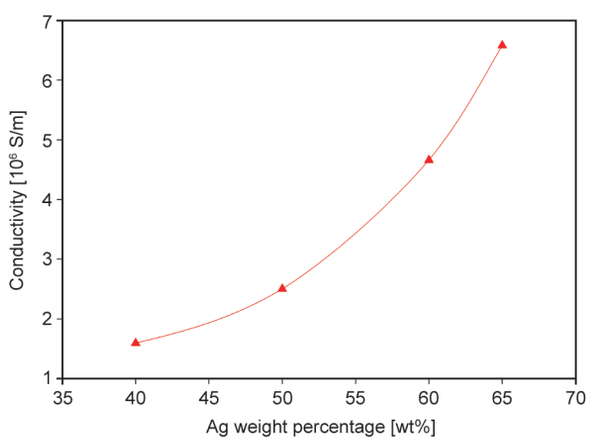

Figure 2. Variation of conductivity at different Ag weight percentages.

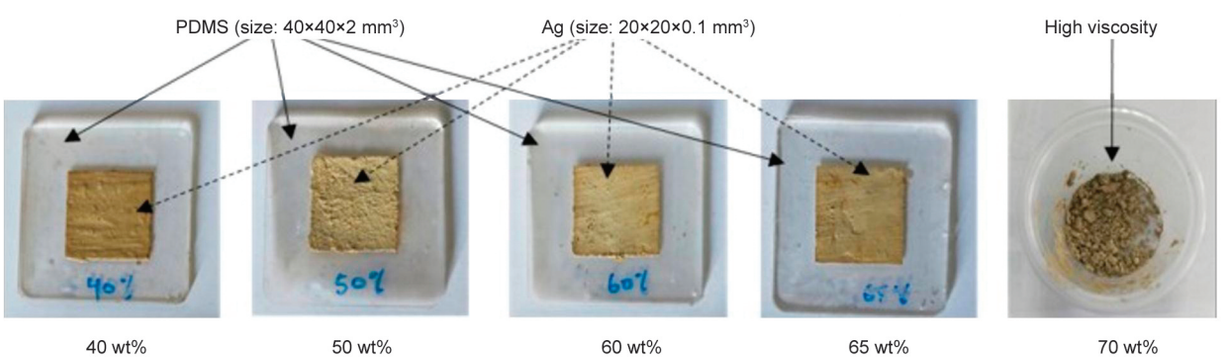

Figure 1. Ag-PDMS paste with different Ag filler loading and 70 wt% Ag is not fabricated due to the high viscosity.

antenna calculated using the measured parameter material from Table 1 (Equations (5) and (6)):

$$W = \frac{c}{2f_r}\frac{1}{\sqrt{\frac{\varepsilon_r}{2}}} \tag{5}$$

$$L = \frac{c}{2f_r\sqrt{\varepsilon_{eff}}} - 2\Delta L \tag{6}$$

where c is the free space velocity, f_r is the resonant frequency, and ε_r is the dielectric constant of the substrate. By considering the fringing field effect, the width and length of the patch at the resonant frequency were determined using Equations (5) and (6), respectively. The ε_{eff} is the effective dielectric constant of substrate material which can be defined as Equation (7):

$$\varepsilon_{eff} = \frac{\varepsilon_r + 1}{2} + \frac{\varepsilon_r - 1}{2}\frac{1}{\sqrt{1 + 12\frac{h}{W}}} \tag{7}$$

where h is the substrate thickness, while the additional ΔL is caused by the fringing field at the radiating edge, given by Equation (8):

$$\Delta L = h \cdot 0.412\frac{\left(\varepsilon_{r_{eff}} + 0.3\right)\left(\frac{W}{h} + 0.264\right)}{\left(\varepsilon_{r_{eff}} - 0.258\right)\left(\frac{W}{h} + 0.8\right)} \tag{8}$$

The initial parameters obtained from the calculated formula were then used to design, simulate, and optimise the rectangular patch antenna using Computer Simulation Technology (CST) software before being fabricated as a prototype. A 65 wt% Ag was used as conductivity ($\sigma = 6.58 \cdot 10^6$ S/m) for the antenna patch and ground. Meanwhile, the dielectric constant, $\varepsilon_r' = 2.74$, and loss tangent, $\tan\delta = 0.057$, at 3.5 GHz of PDMS are used as substrates. The optimised dimensions of PDMS substrate were 60×60 mm^2 with a 2 mm thickness, fully ground at the back with a 0.1 mm thickness, and the patch antenna was 39×24.15 mm^2 with a 0.1-mm thickness. The detailed dimension of the proposed antenna is illustrated in Figures 3a and 3b.

The fabrication of the prototype antenna applied a similar process as the fabrication of the conductive sample illustrated in Sections 2.1 and 2.2. A cutting printer, Silhouette Cameo 3, was used to cut transparent stickers at 0.1 mm thickness (acting as a stencil) accordingly, which followed the patch antenna dimension. The cut patch antenna dimension stickers were then placed on the PDMS substrate to squeegee print the silver paste. The stencil sticker was removed after the squeegee was printed and ready for curing. The same technique was applied to print the conductive paste and ground plane antenna. A coaxial cable-type radio frequency (*RF*), also known as SubMiniature version A (SMA), was connected to the edge feed line of the patch antenna. The silver conductive epoxy adhesive 8330S obtained from M.G. Chemicals (Burlington, Canada) consisted of two components, silver and adhesive were mixed in equal amounts before being applied as an adhesive between the SMA and antenna. The whole antenna package was then thermally cured at 65 °C for two hours to provide an SMA for strong adherence to the stretchable antenna. The fabricated prototype of microstrip patch wearable antenna are illustrated in Figures 3c and 3d.

3. Experimental results and discussion

3.1. Antenna simulation vs. prototype

The simulated PDMS antenna performances using CST software were compared with the prototype. The reflection coefficient, *S11*, for the prototype antenna was obtained using a N5245A type vector network

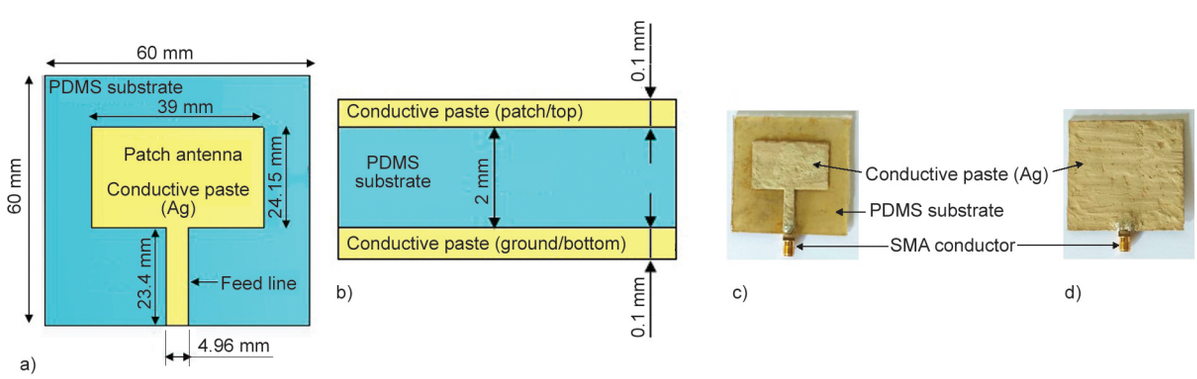

Figure 3. Dimension and prototype of the rectangular patch antenna: a) top view dimension; b) side view dimension; c) top view patch antenna (prototype); and d) back view ground plane antenna (prototype).

analyzer (VNA) from Agilent Technologies inc. (Santa Clara, USA). The antenna tested was connected to the VNA port 1 via coaxial cable to measure the S-parameters (*S11*), resonant frequency, and bandwidth. Figure 4a shows the comparison of *S11* between the simulated and measured antennas. The antenna performed best when the *S11* was below –10 dB, where 90% of the power was transmitted, and the bandwidth was calculated from the lower frequency to the upper frequency of *S11* < –10 dB [63]. The measured resonant frequency prototype antenna was 3.5 GHz, which was similar to the simulated value. However, *S11* measured (–22.32 dB) was better than the simulated (–19.89 dB), indicating that the fabricated antenna was better matched with 50 Ω input impedance [64]. The bandwidth for the simulated and measured antenna was 285 and 196 MHz, respectively. The measurements of the prototype antenna radiation pattern, directivity, and gain were done using an anechoic chamber and Programmable Network Analyser PNA (E83268) from Agilent Technologies (Santa Clara, USA). Figure 4b illustrates the plotted normalized radiation pattern simulated and measured in the *x-z* plane. The main lobe in the upper graph (Figure 4b) implied the antenna was operated in a directional pattern at the front antenna and minor lobe radiation at the back. The three-dimensional (3D) simulated radiation pattern in Figure 4c showed as 360 ° angle of the antenna radiation properties as a function of space coordinated in terms of directivity strength. The directivity of the simulated and measured antenna was 7.45 and 7.7 dBi, respectively. The directivity of an antenna is defined as the ratio of the radiation intensity in a given direction from the antenna to the radiation intensity averaged over all directions [63]. The performance of the antenna can also

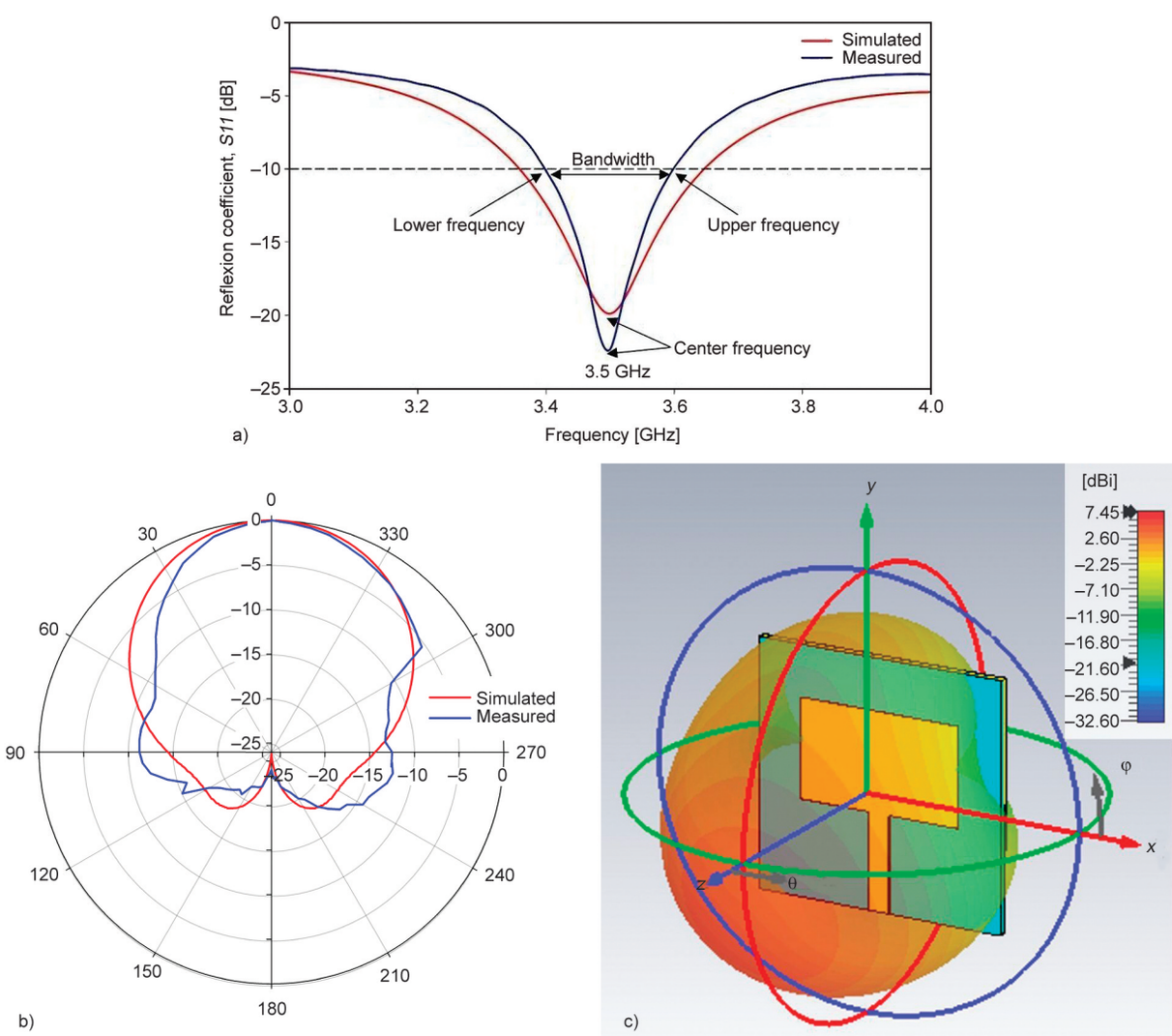

Figure 4. a) Reflection coefficient, *S11* simulated and measured; b) normalized *x-z* plane of radiation pattern simulated and measured; and c) 3D simulated radiation pattern of the simulated and measured antennas.

be measured by the gain that represents the efficiency of the antenna operating at the desired resonant frequency. The antenna gained in this work for simulated and measured was 2.16 and 2.61 dBi, respectively, which had a similar gain average (1–3 dBi) with other reports that used PDMS as a substrate [44, 48, 65].

3.2. Antenna stretching analysis

A mechanical test of stretching the antenna prototype was carried out using the fixture, as illustrated in Figure 5. The stretch analysis was performed at 5 and 10% stretch for the simulated and measured. During stretching, the antenna length will increase, and the thickness will decrease consequently. Meanwhile, the width and volume of the antenna were fixed either with the antenna stretched or not. Thus, by using the volume formula (volume = width × length × thickness), a new dimension of the antenna stretch can be obtained. The antenna was then redesigned in the CST software by increasing the length from the original size to 5 and 10% stretch, as well as decreasing in thickness accordingly. Figure 6a shows the simulated and measured resonance frequency that shifted to the lower frequency when the antenna was stretched. Apparently, the effect of stretching the antenna that led to the decrease in resonant frequency is expected due to the nature of the microstrip patch antenna. This corresponds to Equation (9) [50]:

$$f_r = \frac{c}{2L\sqrt{\varepsilon_{eff}}} \tag{9}$$

where f_r is the resonant frequency, c is the free space velocity, L is the patch length, and ε_{eff} is the effective dielectric constant. The observation is consistent with previous studies [66–68], where an empirical-analytical equation showed that the resonance frequency varies inversely proportional to the electrical length along the direction of current flow on the patch antenna. In other words, as the total electrical size of the antenna stretching increases, the wavelength will increase accordingly, resulting in a lower resonant frequency.

The directivity and gain of the antenna stretching are presented in Figure 6b. In the initial state (0% stretching), the measured directivity antenna was 7.7 dBi and stretching 5 and 10% along its x-axis resulting in a significant decrease to 7.6 and 7.46 dBi, respectively. The same pattern occurred to antenna gain, where the measured antenna without stretching, 2.62 dBi, slightly declined to 2.29 and 2.09 dBi when the antenna stretched at 5 and 10%, correspondingly. The decrease in antenna performance during stretching is mainly because of the piezoresistive effect. In this condition, the electrical resistivity of the material changed when a mechanical strain was applied. During stretching, dislocation of the conductive filler breaks the conductive pathways causing separation of the conductive filler further from each other, which resulted in decreased conductivity [50]. The destruction of the

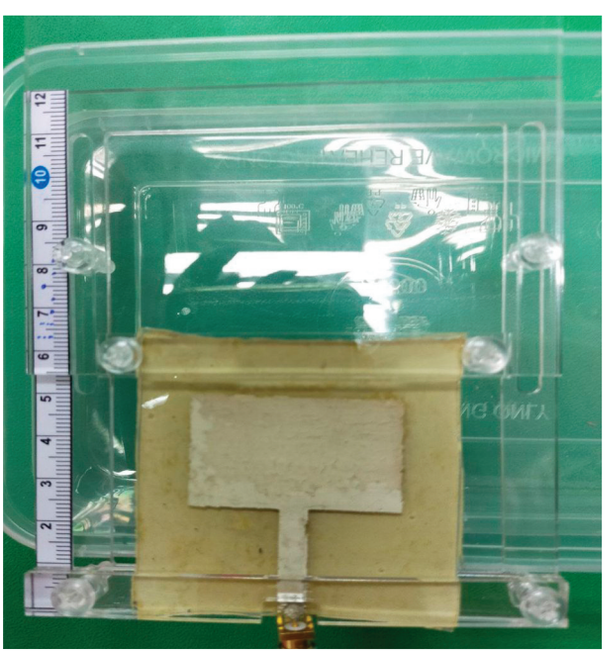

Figure 5. Fixture to stretch the prototype antenna.

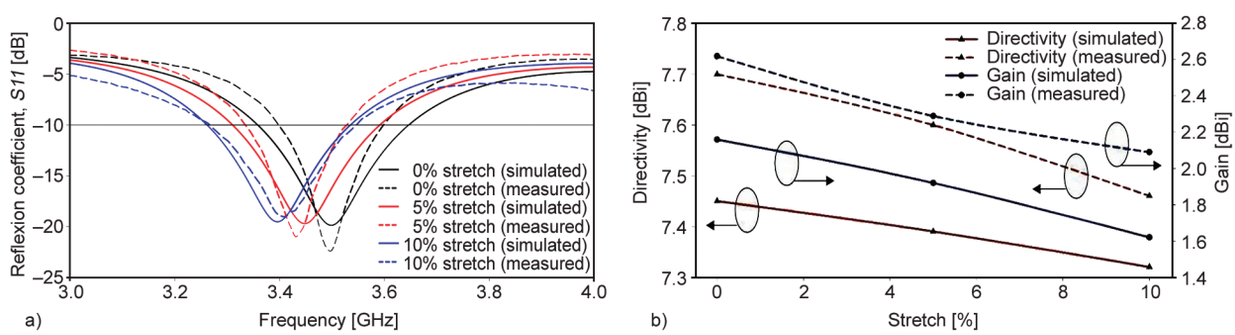

Figure 6. a) Reflection coefficient, *S11* of antenna stretching. b) Directivity and gain of antenna stretching.

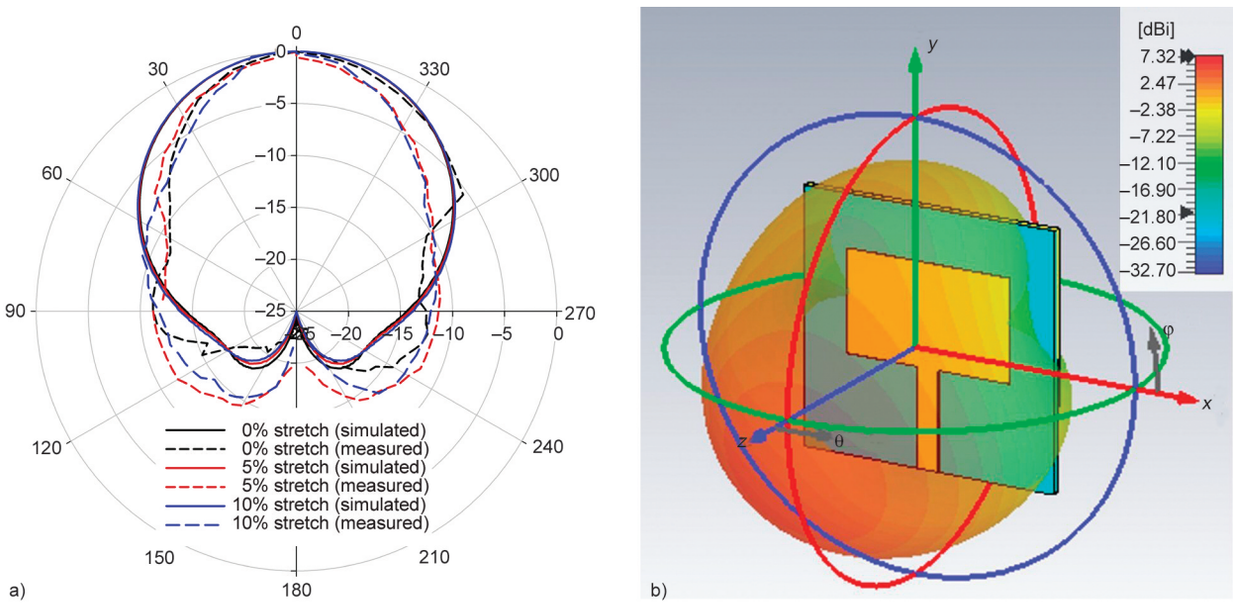

Figure 7. a) Normalized radiation pattern of stretching antenna; and b) 3D simulated radiation pattern of antenna at 10%. stretching.

conductive path leads to a decrease in conductivity at the onset of stretching, which is also shown in several studies [60, 69, 70]. Consequently, the decrease of conductivity when the antenna is stretching affected the reduction of antenna gain performances [71]. Figure 7a illustrates the plotted normalized radiation pattern of antenna stretching simulated, and measured results are in good agreement. The antenna measured radiation behaviour during stretching showed a forward directivity, similar to the antenna without stretching. Meanwhile, there was an insignificant difference in the 3D radiation pattern when the antenna was stretching (Figure 7b).

3.3. Bending analysis

Ideally, the wearable antenna should be attached to the user's forearm. Consequent to the flexibility of the antenna, some antenna deformation is expected. For this reason, the antenna bending analysis was measured at three different angles (21, 30, and 40°), as there are different arm sizes for adults, teenagers, and/or children [72]. A cylinder structure was used in the CST simulation to bend the antenna as a representative model of the human arm. The outer radius of the cylinder can be calculated using Equation (10):

$$S = r\theta \tag{10}$$

where S is the arc length, r is the radius of the circle, and θ is the measured central angle in radian. Since the antenna was made to bend along the x-axis, the antenna's width was used in the calculation as the arc length, as shown in Figure 8a. The antenna bent was designed and simulated using the CST software,

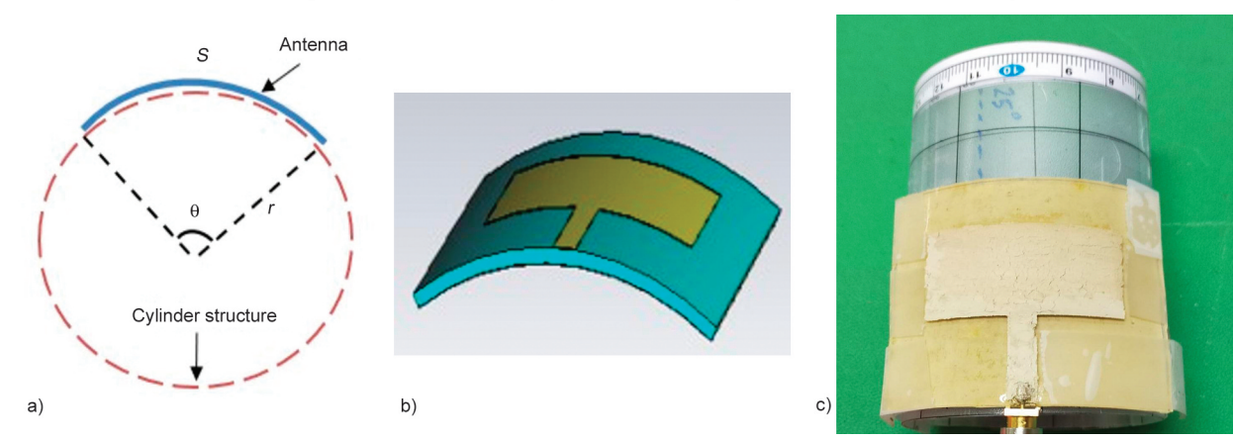

Figure 8. a) Cylindrical- rectangular patch cavity model for patch antenna bent on cylinder surface; b) antenna bent in CST simulation software; and c) the bent antenna prototype.

as illustrated in Figure 8b. The prototype antenna was also tested under several bending angles to emphasise its suitability for conformal wearable systems. It was done by wrapping the wearable antenna around a plastic cylinder, mimicking the bending when the antenna was deployed on a human arm, as shown in Figure 8c. The simulated and measured reflection coefficient indicated in Figure 9a showed the shifted resonance towards the lower frequency when the antenna was bending. Generally, this was due to the changing structure of the antenna in the bent form that affected the surface current flow. The surface current path was elongated when the antenna bending along the *x*-axis increased the wavelength, consequently leading to a lower resonant frequency. The antenna bending analysis was shifted to a lower frequency and was verified by referring to other works [73–75]. The simulated and measured antenna directivity as well as gain at different bending angles is demonstrated in Figure 9b. It was observed that the gain and directivity decreased concurrently when the antenna bent at 21 and 40°. Meanwhile, the observation was vice versa when the antenna bent at 30° angle. The radiation pattern measurement of the wearable antenna in bending conditions compared with simulation are plotted in Figure 9c. The bending antenna that performed forward directional radiation was slightly identical to the antenna in a flat condition. Meanwhile, the back lobe of the antenna radiation was slightly increased when the antenna was bent. The 3D radiation pattern antenna bending at 40° is shown in Figure 9d, which shows a retained radiation shape due to a slightly lower directivity of the antenna without bending.

3.4. Specific absorption rate (*SAR*) analysis

As the antenna was attached to the human body arm, the safety issue was investigated. For that reason, the *SAR* analysis was simulated in CST software using a Hugo human model, where the antenna was placed on the middle-arm, as shown in Figure 10. *SAR* is the measurement that indicates the amount

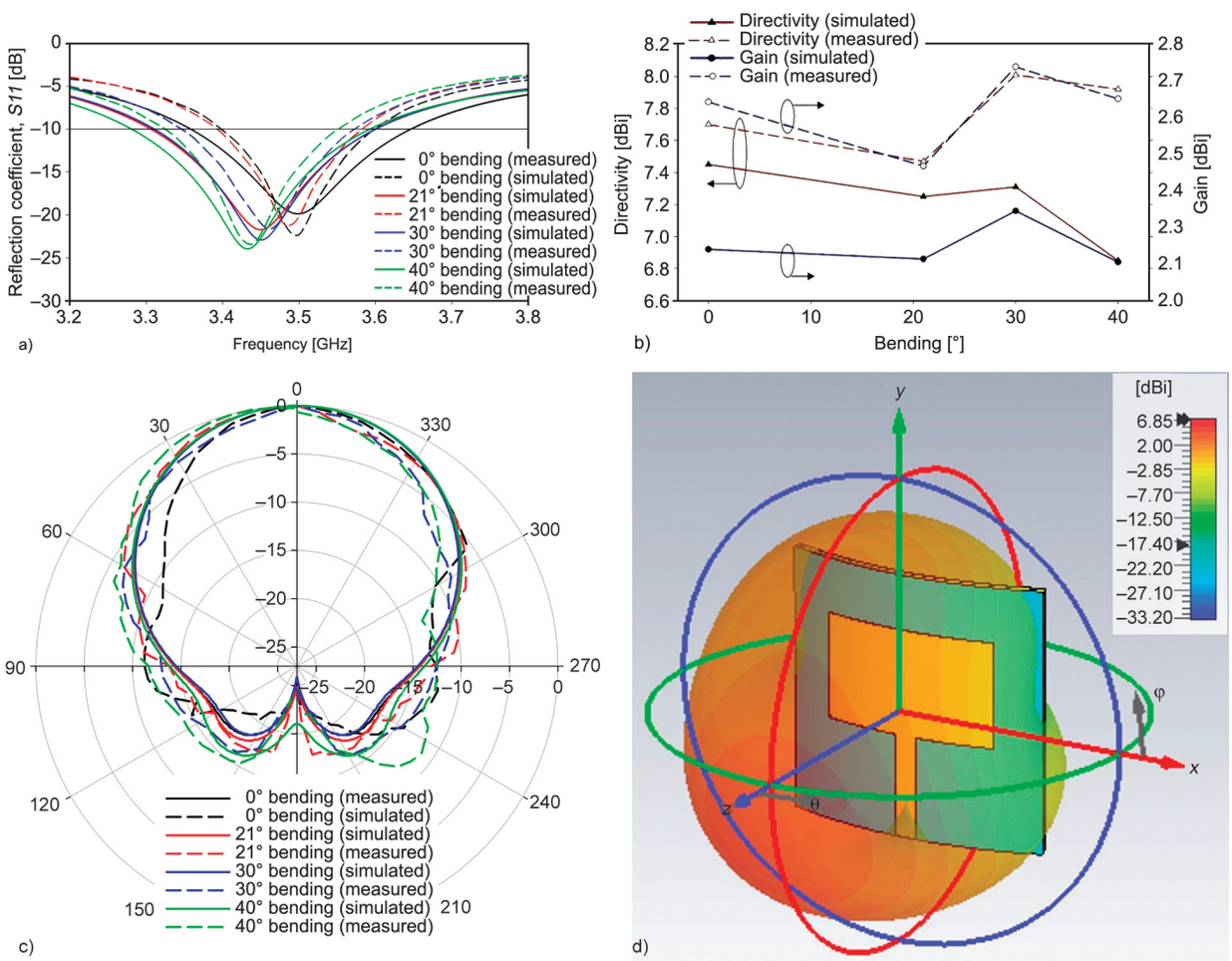

Figure 9. a) Reflection coefficient, *S11* of antenna bending. b) Directivity and gain of antenna bending. c) Normalized radiation pattern antenna. d) 3D simulated radiation pattern antenna at 40° bending.

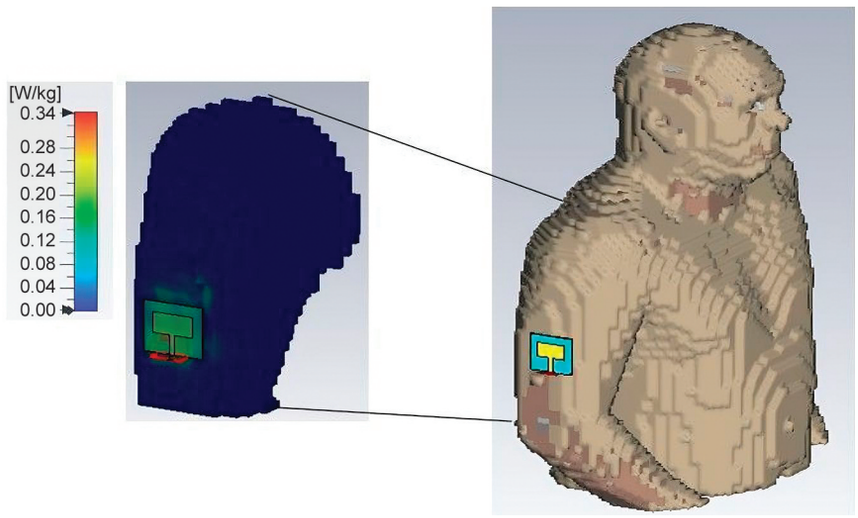

Figure 10. The simulated specific absorption rate (*SAR*) of antenna purposes.

of electromagnetic (EM) power produced by the antenna that is absorbed by the human body. *SAR* is expressed as the absorbed power per unit of tissue mass and its unit is W/kg [76]. The maximum *SAR* value for the purpose antenna was 0.34 W/kg for 1 g of tissue at a resonance frequency of 3.5 GHz. The *SAR* value was very low compared to the maximum limit of 1.6 W/kg identified in IEEE standard safety levels for human exposure to radiofrequency electromagnetic fields, which ranges from 3 kHz to 300 GHz (IEEE std C95.1-1991) [77].

4. Conclusions

A stretchable and bendable conductive ink paste was developed based on the polysiloxane composite and silver particles as the conductive filler. Four different samples of silver powder wt% were made with PDMS as a substrate. The higher silver wt% showed better conductivity. The proof-of-concept prototype microstrip patch antenna was designed and fabricated at a resonance frequency of 3.5 GHz with a reflection coefficient below –19 dB. The bandwidth was 196 MHz in its initial state but was subsequently decreased slightly during its stretching at 5 and 10% with 188 and 270 MHz, respectively. However, the bandwidth antenna with bending consistently increased compared to the antenna without bending. The antenna performances reflected the directivity and gain, which slightly fluctuated when the antenna was stretching and when bending was reasonable. Meanwhile, the antenna radiation pattern maintained the forward directional radiation pattern at the front of the antenna and minor lobe radiation at the back when the antenna stretched and bent. Additionally, the *SAR* value of the antenna was 0.34 W/kg for 1 g of tissue, which was far less than the maximum limit (1.6 W/kg) of the standard safety level for humans that are exposed to electromagnetic radio frequency. The *SAR* analysis showed the conductive polymer antenna was safe to be used on the human body as well as its ability to undergo stretching and bending, which would make it an attractive candidate for antenna wearable 5G applications, implanted medical devices, and body sensor networks.

Acknowledgements

The authors would like to thank Universiti Sains Malaysia for the financial support provided through the Research University (RUI) grant (Ref. No.: 6071429).

References

[1] Halary J., Cookson P., Stanford J. L., Lovell P. A., Young R. J.: Smart nanostructured polymeric coatings for use as remote optical strain sensors. Advanced Engineering Materials, **6**, 729–733 (2004). https://doi.org/10.1002/adem.200400061

[2] Genchi G. G., Marino A., Grillone A., Pezzini I., Ciofani G.: Remote control of cellular functions: The role of smart nanomaterials in the medicine of the future. Advanced Healthcare Materials, **6**, 1700002 (2017). https://doi.org/10.1002/adhm.201700002

[3] Chow W. S., Mohd Ishak Z. A.: Smart polymer nanocomposites: A review. Express Polymer Letters, **14**, 416–435 (2020). https://doi.org/10.3144/expresspolymlett.2020.35

[4] Meng H., Hu J.: A brief review of stimulus-active polymers responsive to thermal, light, magnetic, electric, and water/solvent stimuli. Journal of Intelligent Material Systems and Structures, **21**, 859–885 (2010). https://doi.org/10.1177/1045389X10369718

[5] Basak S., Bandyopadhyay A.: Tethering smartness to the metal containing polymers – Recent trends in the stimuli-responsive metal containing polymers. Journal of Organometallic Chemistry, **956**, 122129 (2021). https://doi.org/10.1016/j.jorganchem.2021.122129

[6] Hager M. D., Bode S., Weber C., Schubert U. S.: Shape memory polymers: Past, present and future developments. Progress in Polymer Science, **49–50**, 3–33 (2015). https://doi.org/10.1016/j.progpolymsci.2015.04.002

[7] Pilate F., Toncheva A., Dubois P., Raquez J-M.: Shape-memory polymers for multiple applications in the materials world. European Polymer Journal, **80**, 268–294 (2016). https://doi.org/10.1016/j.eurpolymj.2016.05.004

[8] Luo H., Li C., Shi C., Nie S., Song J.: Switchable dry adhesive based on shape memory polymer with hemispherical indenters for transfer printing. Theoretical and Applied Mechanics Letters, **11**, 100308 (2021). https://doi.org/10.1016/j.taml.2021.100308

[9] Liu Y. D., Choi H. J.: Recent progress in smart polymer composite particles in electric and magnetic fields. Polymer International, **62**, 147–151 (2013). https://doi.org/10.1002/pi.4441

[10] Jaafar M. F., Mustapha F., Mustapha M.: Review of current research progress related to magnetorheological elastomer material. Journal of Materials Research and Technology, **15**, 5010–5045 (2021). https://doi.org/10.1016/j.jmrt.2021.10.058

[11] Shen F., Kang G., Lam Y. C., Liu Y., Zhou K.: Thermo-elastic-viscoplastic-damage model for self-heating and mechanical behavior of thermoplastic polymers. International Journal of Plasticity, **121**, 227–243 (2019). https://doi.org/10.1016/j.ijplas.2019.06.003

[12] Katunin A., Wachla D.: Minimizing self-heating based fatigue degradation in polymeric composites by air cooling. Procedia Structural Integrity, **18**, 20–27 (2019). https://doi.org/10.1016/j.prostr.2019.08.136

[13] Formisano A., Lambiase F., Durante M.: Polymer self-heating during incremental forming. Journal of Manufacturing Processes, **58**, 1189–1199 (2020). https://doi.org/10.1016/j.jmapro.2020.09.031

[14] Saeedi A., Shokrieh M. M.: A novel self-healing composite made of thermally reversible polymer and shape memory alloy reinforcement. Journal of Intelligent Material Systems and Structures, **30**, 1585–1593 (2019). https://doi.org/10.1177/1045389X19844015

[15] Nam J., Jang W., Rajeev K. K., Lee J-H., Kim Y., Kim T-H.: Ion-conductive self-healing polymer network based on reversible imine bonding for Si electrodes. Journal of Power Sources, **499**, 229968 (2021). https://doi.org/10.1016/j.jpowsour.2021.229968

[16] Cherupurakal N., Mozumder M. S., Mourad A-H. I., Lalwani S.: Recent advances in superhydrophobic polymers for antireflective self-cleaning solar panels. Renewable and Sustainable Energy Reviews, **151**, 111538 (2021). https://doi.org/10.1016/j.rser.2021.111538

[17] Mi Y., Wang N., Fang X., Cao J., Tao M., Cao Z.: Interfacial polymerization nanofiltration membrane with visible light photocatalytic self-cleaning performance by incorporation of CQD/TiO_2. Separation and Purification Technology, **277**, 119500 (2021). https://doi.org/10.1016/j.seppur.2021.119500

[18] Asar A., Irfan M. S., Khan K. A., Zaki W., Umer R.: Self-sensing shape memory polymer composites reinforced with functional textiles. Composites Science and Technology, **221**, 109219 (2021). https://doi.org/10.1016/j.compscitech.2021.109219

[19] Roche S., Ibarz G., Crespo C., Chiminelli A., Araujo A., Santos R., Zhang Z., Li X., Dong H.: Self-sensing polymeric materials based on fluorescent microcapsules for the detection of microcracks. Journal of Materials Research and Technology, **16**, 505–515 (2022). https://doi.org/10.1016/j.jmrt.2021.11.014

[20] Han J., Kim J. H., Choi H. J., Kim S. W., Sung S. M., Kim M. S., Choi B. K., Paik J. H., Lee J. S., Cho Y. S.: Origin of enhanced piezoelectric energy harvesting in all-polymer-based core–shell nanofibers with controlled shell-thickness. Composites Part B: Engineering, **223**, 109141 (2021). https://doi.org/10.1016/j.compositesb.2021.109141

[21] Cao Y., Meng Y., Jiang Y., Qian S., Fan D., Zhou X., Qian Y., Lin S., Qian T., Pan Q.: Healable supramolecular phase change polymers for thermal energy harvesting and storage. Chemical Engineering Journal, **433**, 134549 (2022). https://doi.org/10.1016/j.cej.2022.134549

[22] Roopa J., Swathi H., Geetha K. S., Satyanaryana B. S.: Modeling and simulation of triboelectric nanogenerator for energy harvesting using COMSOL Multiphysics® and optimization on thickness of flexible polymer. Materials Today: Proceedings, **48**, 702–705 (2022). https://doi.org/10.1016/j.matpr.2021.10.128

[23] Rivero R. E., Molina M. A., Rivarola C. R., Barbero C. A.: Pressure and microwave sensors/actuators based on smart hydrogel/conductive polymer nanocomposite. Sensors and Actuators B: Chemical, **190**, 270–278 (2014). https://doi.org/10.1016/j.snb.2013.08.054

[24] Song S., Zhang C., Wang J., Li W., Jiang Z., Zhang Y.: High-performance nacre-like graphene@polymer supported montmorillonite composite actuator and sensor. Sensors and Actuators B: Chemical, **332**, 129446 (2021). https://doi.org/10.1016/j.snb.2021.129446

[25] Vidal R., Moliner E., Martin P. P., Fita S., Wonneberger M., Verdejo E., Vanfleteren F., Lapeña N., González A.: Life cycle assessment of novel aircraft interior panels made from renewable or recyclable polymers with natural fiber reinforcements and non-halogenated flame retardants. Journal of Industrial Ecology, **22**, 132–144 (2018). https://doi.org/10.1111/jiec.12544

[26] Bashir M., Rajendran P.: A review on electroactive polymers development for aerospace applications. Journal of Intelligent Material Systems and Structures, **29**, 3681–3695 (2018).
https://doi.org/10.1177/1045389X18798951

[27] Jayalakshmi C. G., Inamdar A., Anand A., Kandasubramanian B.: Polymer matrix composites as broadband radar absorbing structures for stealth aircrafts. Journal of Applied Polymer Science, **136**, 47241 (2019).
https://doi.org/10.1002/app.47241

[28] Trung T. Q., Lee N-E.: Recent progress on stretchable electronic devices with intrinsically stretchable components. Advanced Materials, **29**, 1603167 (2017).
https://doi.org/10.1002/adma.201603167

[29] Kim D. W., Kong M., Jeong U.: Interface design for stretchable electronic devices. Advanced Science, **8**, 2004170 (2021).
https://doi.org/10.1002/advs.202004170

[30] Song C., Chen B., Hwang J., Lee S., Suo Z., Ahn H.: A printed highly stretchable supercapacitor by a combination of carbon ink and polymer network. Extreme Mechanics Letters, **49**, 101459 (2021).
https://doi.org/10.1016/j.eml.2021.101459

[31] Alqadami A. S. M., Bialkowski K. S., Mobashsher A. T., Abbosh A. M.: Wearable electromagnetic head imaging system using flexible wideband antenna array based on polymer technology for brain stroke diagnosis. IEEE Transactions on Biomedical Circuits and Systems, **13**, 124–134 (2019).
https://doi.org/10.1109/TBCAS.2018.2878057

[32] Mokhtari F., Spinks G. M., Fay C., Cheng Z., Raad R., Xi J., Foroughi J.: Wearable electronic textiles from nanostructured piezoelectric fibers. Advanced Materials Technologies, **5**, 1900900 (2020).
https://doi.org/10.1002/admt.201900900

[33] Afroj S., Tan S., Abdelkader A. M., Novoselov K. S., Karim N.: Highly conductive, scalable, and machine washable graphene-based E-textiles for multifunctional wearable electronic applications. Advanced Functional Materials, **30**, 2000293 (2020).
https://doi.org/10.1002/adfm.202000293

[34] Liman M. L. R., Islam M. T., Hossain M. M.: Mapping the progress in flexible electrodes for wearable electronic textiles: Materials, durability, and applications. Advanced Electronic Materials, **8**, 2100578 (2022).
https://doi.org/10.1002/aelm.202100578

[35] Paracha K. N., Abdul Rahim S. K., Soh P. J., Khalily M.: Wearable antennas: A review of materials, structures, and innovative features for autonomous communication and sensing. IEEE Access, **7**, 56694–56712 (2019).
https://doi.org/10.1109/ACCESS.2019.2909146

[36] Kirtania S. G., Elger A. W., Hasan M. R., Wisniewska A., Sekhar K., Karacolak T., Sekhar P. K.: Flexible antennas: A review. Micromachines, **11**, 847 (2020).
https://doi.org/10.3390/mi11090847

[37] Ali S. M., Sovuthy C., Imran M. A., Socheatra S., Abbasi Q. H., Abidin Z. Z.: Recent advances of wearable antennas in materials, fabrication methods, designs, and their applications: State-of-the-art. Micromachines, **11**, 888 (2020).
https://doi.org/10.3390/mi11100888

[38] Aun N. F. M., Soh P. J., Al-Hadi A. A., Jamlos M. F., Vandenbosch G. A. E., Schreurs D. S.: A revolutionizing wearable for 5G: 5G technologies: Recent developments and future perspectives for wearable devices and antennas. IEEE Microwave Magazine, **18**, 108–124 (2017).
https://doi.org/10.1109/MMM.2017.2664019

[39] Isa M. S. M., Azmi A. N. L., Isa A. A. M., Zin M. S. I. M., Saat M. S. M., Zakaria Z., Abu M., Ahmad A.: Comparative study of mutual coupling on microstrip antennas for wireless local area network (WLAN) application. Journal of Telecommunication, Electronic and Computer Engineering, **7**, 161–167 (2015).

[40] Ali S. M., Sovuthy C., Imran M. A., Socheatra S., Abbasi Q. H., Abidin Z. Z.: Recent advances of wearable antennas in materials, fabrication methods, designs, and their applications: State-of-the-art. Micromachines, **11**, 888 (2020).
https://doi.org/10.3390/mi11100888

[41] Singh A., Kaur G., Kalra P., Kaur A., Singh J., Pandey P., Sidhu E.: Design and performance analysis of rectangular textile microstrip patch antennas employing different textile materials for Ku band applications. in '2017 Progress in Electromagnetics Research Symposium, St Petersburg, Russia' 516–522 (2017).
https://doi.org/10.1109/PIERS.2017.8261795

[42] Sharma D., Dubey S. K., Ojha V. N.: Wearable antenna for millimeter wave 5G communications. in '2018 IEEE Indian Conference on Antennas and Propagation (InCAP), Hyderabad, India' 1–4 (2018).
https://doi.org/10.1109/INCAP.2018.8770921

[43] Lajevardi M. E., Kamyab M.: Ultraminiaturized metamaterial-inspired SIW textile antenna for off-body applications. IEEE Antennas and Wireless Propagation Letters, **16**, 3155–3158 (2017).
https://doi.org/10.1109/LAWP.2017.2766201

[44] Sayem A. S. M., Simorangkir R. B. V. B., Esselle K. P., Hashmi R. M.: Feasibility study of PDMS embedded transparent conductive fabric for the realization of transparent flexible antennas. in '13th European Conference on Antennas and Propagation (EuCAP 2019), Krakow, Poland' 1–4 (2019).

[45] Simorangkir R. B. V. B., Yang Y., Esselle K. P.: Robust implementation of flexible wearable antennas with PDMS-embedded conductive fabric. in '12th European Conference on Antenna and Propagation (EuCAP 2018), London, United Kingdom' 12–16 (2018).
https://doi.org/10.1049/cp.2018.0846

[46] Alqadami A. S. M., Jamlos M. F., Soh P. J., Vandenbosch G. A. E.: Assessment of PDMS technology in a MIMO antenna array. IEEE Antennas and Wireless Propagation Letters, **15**, 1939–1942 (2016). https://doi.org/10.1109/LAWP.2015.2513960

[47] Joshi R., Constantinides C., Podilchak S. K., Ramli M. N., Lago H., Soh P. J.: Robust and compact PDMS antennas for search and rescue operations and emergency communications. in '12th European Conference on Antenna and Propagation (EuCAP 2018), London, United Kingdom' 1–5 (2018). https://doi.org/10.1049/cp.2018.0975

[48] Lin C-P., Chang C-H., Cheng Y. T., Jou C. F.: Development of a flexible SU-8/PDMS-based antenna. IEEE Antennas and Wireless Propagation Letters, **10**, 1108–1111 (2011). https://doi.org/10.1109/LAWP.2011.2170398

[49] Dow Chemical Company.: SYLGARD TM 184 silicone elastomer technical datasheet. Silicone elastomer data sheet (2017).

[50] Ramli M. R., Ibrahim S., Ahmad Z., Abidin I. S. Z., Ain M. F.: Stretchable conductive ink based on polysiloxane-silver composite and its application as a frequency reconfigurable patch antenna for wearable electronics. ACS Applied Materials and Interfaces, **11**, 28033–28042 (2019). https://doi.org/10.1021/acsami.9b07671

[51] Sharma P. K., Gupta N., Dankov P. I.: Analysis of dielectric properties of polydimethylsiloxane (PDMS) as a flexible substrate for sensors and antenna applications. IEEE Sensors Journal, **21**, 19492–19504 (2021). https://doi.org/10.1109/JSEN.2021.3089827

[52] Dankov P. I., Sharma P. K., Gupta N.: Numerical and experimental investigation of the opposite influence of dielectric anisotropy and substrate bending on planar radiators and sensors. Sensors, **21**, 16 (2021). https://doi.org/10.3390/s21010016

[53] Bakar A. A., Hasnan F., Razali A. R., Rahim A. F. A., Osman M. S., Ali T., Radzali R.: Polydimethylsiloxane as a potential antenna substrate. Acta Physica Polonica A, **135**, 938–941 (2019). https://doi.org/10.12693/APhysPolA.135.938

[54] Zhao T., Hou C., Zhang H., Zhu R., She S., Wang J., Li T., Liu Z., Wei B.: Electromagnetic wave absorbing properties of amorphous carbon nanotubes. Scientific Reports, **4**, 5619 (2014). https://doi.org/10.1038/srep05619

[55] Sun L., Park S. S., Sheberla D., Dincă M.: Measuring and reporting electrical conductivity in metal-organic frameworks: Cd_2(TTFTB) as a case study. Journal of the American Chemical Society, **138**, 14772–14782 (2016). https://doi.org/10.1021/jacs.6b09345

[56] Rizwan M., Khan M. W. A., Sydänheimo L., Virkki J., Ukkonen L.: Flexible and stretchable brush-painted wearable antenna on a three-dimensional (3-D) printed substrate. IEEE Antennas and Wireless Propagation Letters, **16**, 3108–3112 (2017). https://doi.org/10.1109/LAWP.2017.2763743

[57] Song L., Myers A. C., Adams J. J., Zhu Y.: Stretchable and reversibly deformable radio frequency antennas based on silver nanowires. ACS Applied Materials and Interfaces, **6**, 4248–4253 (2014). https://doi.org/10.1021/am405972e

[58] Saghlatoon H., Mahdi M. H., Mirzavand R., Mousavi P., Kumar A., La T. G., Chung H-J.: A novel investigation on printed stretchable WLAN antennas. in '2017 IEEE International Symposium Antennas and Propagation and USNC/URSI National Radio Science Meeting, San Diego, USA' 2537–2538 (2017). https://doi.org/10.1109/APUSNCURSINRSM.2017.8073311

[59] Rahman H. A., Rahim S. K. A., Abedian M., Najib N.: Design of a flexible antenna using printed silver loaded epoxy on PDMS/plastic substrate for wearable applications. in '10th European Conference on Antennas and Propagation, EuCAP 2016, Davos, Switzeland' 1–4 (2016). https://doi.org/10.1109/EuCAP.2016.7481327

[60] Chen Z., Xi J., Huang W., Yuen M. M. F.: Stretchable conductive elastomer for wireless wearable communication applications. Scientific Reports, **7**, 10958 (2017). https://doi.org/10.1038/s41598-017-11392-w

[61] Hafeez H., Ryu H-Y., Paluvai N. R., Park J-G.: Conductive and transparent submicron polymer lens array fabrication for electrowetting applications. Journal of Adhesion Science and Technology, **32**, 1975–1986 (2018). https://doi.org/10.1080/01694243.2018.1461447

[62] Liang G. D., Tjong S. C.: Electrical properties of percolative polystyrene/carbon nanofiber composites. IEEE Transactions on Dielectrics and Electrical Insulation, **15**, 214–220 (2008). https://doi.org/10.1109/T-DEI.2008.4446753

[63] Balanis C. A.: Antenna theory: Analysis and design. Wiley, Hoboken (2005).

[64] Li Z., Le T., Wu Z., Yao Y., Li L., Tentzeris M., Moon K-S., Wong C. P.: Rational design of a printable, highly conductive silicone-based electrically conductive adhesive for stretchable radio-frequency antennas. Advanced Functional Materials, **25**, 464–470 (2015). https://doi.org/10.1002/adfm.201403275

[65] Rahman H. A., Rahim S. K. A.: Dual band PDMS based flexible antenna for wearable application. in 'IEEE MTT-S International Microwave Workshop Series on RF and Wireless Technologies for Biomedical and Healthcare Applications, IMWS-BIO 2015 – Proceedings, Taipei, Taiwan' 193–194 (2015). https://doi.org/10.1109/IMWS-BIO.2015.7303843

[66] Cheng S., Wu Z.: A microfluidic, reversibly stretchable, large-area wireless strain sensor. Advanced Functional Materials, **21**, 2282–2290 (2011). https://doi.org/10.1002/adfm.201002508

[67] Wu Z., Hjort K., Jeong S. H.: Microfluidic stretchable radio-frequency devices. Proceedings of the IEEE, **103**, 1211–1225 (2015). https://doi.org/10.1109/JPROC.2015.2395716

[68] Zhu J., Fox J. J., Yi N., Cheng H.: Structural design for stretchable microstrip antennas. ACS Applied Materials and Interfaces, **11**, 8867–8877 (2019). https://doi.org/10.1021/acsami.8b22021

[69] Feng C., Jiang L. Y.: Investigation of uniaxial stretching effects on the electrical conductivity of CNT-polymer nanocomposites. Journal of Physics D: Applied Physics, **47**, 405103 (2014). https://doi.org/10.1088/0022-3727/47/40/405103

[70] Kim B. S., Shin K-Y., Pyo J. B., Lee J., Son J. G., Lee S-S., Park J. H.: Reversibly stretchable, optically transparent radio-frequency antennas based on wavy Ag nanowire networks. ACS Applied Materials and Interfaces, **8**, 2582–2590 (2016). https://doi.org/10.1021/acsami.5b10317

[71] Tang Q-Y., Pan Y-M., Chan Y-C., Leung K. W.: Frequency-tunable soft composite antennas for wireless sensing. Sensors and Actuators A: Physical, **179**, 137–145 (2012). https://doi.org/10.1016/j.sna.2012.03.024

[72] Fryar C. D., Gu Q., Ogden C. L., Flegal K. M.: Anthropometric reference data for children and adults: United States, (2011–2014). DHHS Publication, National Center for Health Statistics (U.S.), Hyattsville (2016).

[73] Simorangkir R. B. V. B., Yang Y., Matekovits L., Esselle K. P.: Dual-band dual-mode textile antenna on PDMS substrate for body-centric communications. IEEE Antennas and Wireless Propagation Letters, **7**, 677–680 (2017). https://doi.org/10.1109/LAWP.2016.2598729

[74] Haerinia M., Noghanian S.: Study of bending effects on a dual-band implantable antenna. in 'IEEE International Symposium on Antennas and Propagation and USNC-URSI Radio Science Meeting, Atlanta, USA' Vol. 50, 753–754 (2019). https://doi.org/10.1109/APUSNCURSINRSM.2019.8888320

[75] Mersani A., Osman L., Ribero J. M.: Effect of bending on the characteristics of a coplanar textile antenna. in '18th Mediterranean Microwave Symposium, Istanbul, Turkey' 255–257 (2019). https://doi.org/10.1109/MMS.2018.8612049

[76] Yalduz H., Tabaru T. E., Kilic V. T., Turkmen M.: Design and analysis of low profile and low *SAR* full-textile UWB wearable antenna with metamaterial for WBAN applications. AEU – International Journal of Electronics and Communications, **126**, 153465 (2020). https://doi.org/10.1016/j.aeue.2020.153465

[77] IEEE Std C95.1™ – 2005: IEEE standard for safety levels with respect to human exposure to radio frequency electromagnetic fields, 3 kHz to 300 GHz (1999).